8-1-2016

Mechanical Properties of Natural Chitosan/Hydroxyapatite/Magnetite Nanocomposites for Tissue Engineering Applications

Fatemeh Heidari
Yasouj University

Mehdi Razavi
Brunel University

Mohammad E. Bahrololoom
Shiraz University

Reza Bazargan-Lari
Islamic Azad University, Iran

Daryoosh Vashaee
North Carolina State University

See next page for additional authors

Accepted version. *Materials Science and Engineering: C,* Vol. 65 (August 1, 2016): 338-344. DOI.

Mechanical Properties of Natural Chitosan/Hydroxyapatite/Magnetite Nanocomposites for Tissue Engineering Applications

Fatemeh Heidari
Department of Materials Science and Engineering, School of Engineering, Yasouj University,
Yasuj, Iran
Mehdi Razavi
BCAST, Institute of Materials and Manufacturing,
Brunel University London,
Uxbridge, London, UK
Brunel Institute for Bioengineering, Brunel University London,
Uxbridge, London, UK
Mohammad E. Bahrololoom
Department of Materials Science and Engineering,
School of Engineering, Shiraz University,
Shiraz, Iran
Reza Bazargan-Lari
Department of Materials Science and Engineering,
Marvdasht Branch, Islamic Azad University,
Marvdasht, Iran

Materials Science and Engineering C, Vol 65 (August 1, 2016): pg. 338-344. DOI.

Daryoosh Vashaee
Electrical and Computer Engineering Department,
North Carolina State University,
Raleigh, NC
Hari Kotturi
Department of Biology, University of Central Oklahoma,
Edmond, OK
Lobat Tayebi
School of Dentistry, Department of Developmental Sciences,
Marquette University,
Milwaukee, WI
Department of Engineering Science, University of Oxford,
Oxford, UK

Abstract: Chitosan (CS), hydroxyapatite (HA), and magnetite (Fe_3O_4) have been broadly employed for bone treatment applications. Having a hybrid biomaterial composed of the aforementioned constituents not only accumulates the useful characteristics of each component, but also provides outstanding composite properties. In the present research, mechanical properties of pure CS, CS/HA, CS/HA/magnetite, and CS/magnetite were evaluated by the measurements of bending strength, elastic modulus, compressive strength and hardness values. Moreover, the morphology of the bending fracture surfaces were characterized using a scanning electron microscope (SEM) and an image analyzer. Studies were also conducted to examine the biological response of the human Mesenchymal Stem Cells (hMSCs) on different composites. We conclude that, although all of these composites possess in-vitro biocompatibility, adding hydroxyapatite and magnetite to the chitosan matrix can noticeably enhance the mechanical properties of the pure chitosan.
Keywords: Bending, Compressive, Hardness, Hydroxyapatite, Chitosan, Magnetite nano-particles

1. Introduction

In the history of bone grafting, the first successful surgery is credited to the treatment of a soldier's cranial defect using a dog's skull in 1668.[1] Since then, substantial advances have been made including development of various substitute materials containing metals, synthetic and natural polymers, ceramics, hydrogels, and their

composites in the form of bulk or nano-particles.[2,3,4,5,6,7] These materials can be nondegradable such as some metals and polymers, and degradable such as many of hydrogels, ceramics, polymers, and even some recently developed degradable metals.[7,8,9,10,11,12] They can be made to act as implants or scaffolds that guide regeneration of the surrounding tissues towards formation of new bones and treatment of the area of the injury.[13,14] These scaffolds or implants are usually being either body or surface modified by the use of various coatings or nano-particles to tune their characteristics or to add extra functionalities.[15,16,17,18,19]

Chitosan (CS) has been known as a biocompatible polymeric material for orthopedic applications due to its non-toxicity, biodegradability, and wound healing characteristics.[20,21,22,23,24] CS is employed in different shapes such as microspheres,[25] membranes,[26] pins, and rods.[27] As a bioactive ceramic, hydroxyapatite (HA) is extensively used in bone tissue engineering due to its excellent biocompatibility and osteoconductive properties.[28,29,30,31] Moreover, HA is able to help regeneration of the osteoblasts.[28,29,30,31] However, its poor mechanical properties including low fracture toughness and lack of ductility have restricted its clinical applications.[32,33] Making composites of HA with other materials can significantly improve its mechanical and biological properties.[34,35,36] Combination of CS and HA can make a composite with enhanced bioactivity, mechanical properties, and bone bonding ability.[37,38,39,40] Recent investigations have shown that CS/HA composites can facilitate bone remodeling and growth.[41,42]

Bending strength and elastic modulus of human cortical bone are 100–150 MPa and 7–25 GPa, respectively.[43] Consequently, the bone repair materials should ideally possess similar values of bending strength and elastic modulus. However, these values can hardly be achieved in CS/HA composites.[43,44,45] Several factors may contribute to the mechanical properties of these composites. These factors include particle size of HA, the mechanical strength of CS matrix, the interfacial interactions between CS and HA, and good distribution of HA in CS matrix.[46,47]

Adding a third component to the composite, such as PLLA[48] and genipin[43] can change the mechanical properties of the CS/HA composite.

Magnetite with the chemical formula of Fe_3O_4 is a material utilized often to add special functionality to the composites. Moreover, the magnetite is supposed to align the growth of osteoblast cells at presence of an external magnetic field.[49,50] Magnetic resonance imaging (MRI), hyperthermia, and drug-delivery systems are the areas in which magnetite applications are important.[49,51] Furthermore, nano-sized magnetic carriers present superior performance owing to their higher specific surface area and lower internal diffusion resistance compared to the large-sized magnetite particles.[50]

In this work, in particular, natural HA and CS have been utilized instead of synthetic types in the preparation of the composite structures. Natural HA and CS were extracted from the bone and shrimp shells, respectively. Therefore, they are more cost-effective than synthetic HA and CS. Moreover, the magnetic nano-particles were formed distinctively via in-situ precipitation in the CS/HA matrix.

We have recently prepared a CS/HA/magnetite nanocomposite via similar approach.[52] The structural, magnetic and thermal analysis such as Fourier transforms infrared spectroscopy (FTIR), magnetometer hysteresis loop, thermogravimetric analysis (TGA), and differential scanning calorimetry (DSC) have been reported elsewhere.[52] In this work, we further assessed the mechanical properties of this composite material. We present detailed study of the mechanical properties of CS, CS/HA, CS/HA/magnetite, and CS/magnetite samples, such as hardness, bending, and compression. Furthermore, the cyto-compatibilities of these composite materials were evaluated and discussed by the use of human Mesenchymal Stem Cells (hMSCs).

2. Materials and methods

2.1. Material preparation

2.1.1. Chitosan extraction from the shrimp shells

In this study, chitin was extracted from the shrimp shells. The extraction method was performed according to the previous report of Bazargan et al.[53] In this technique, a diluted HCl solution was utilized for demineralization process. For this purpose, the shrimp shell powder (100 g) was added to 1000 ml of 7% (w/w) HCl at room temperature (25 °C) for 24 h. After filtration with a filter paper, the residue was washed with distilled water. The residue was deproteinized by adding the NaOH (1000 ml, 10% (w/w)) at 25 °C for 24 h. Then, the prepared chitin was washed with distilled water. Dehydration process was carried out by the sequential use of 95% and absolute ethanol and finally it was dried at 50 °C overnight.[53] The synthesized chitin was kept in the NaOH solution at 110 °C for 4 h to prepare crude chitosan. After filtration and washing with distilled water at 60 °C, the materials dried overnight at 50 °C in an oven. The degree of deacetylation of chitosan was calculated to be around 75% by the use of the Sabnis's formula.[54]

2.1.2. Hydroxyapatite extraction from the bovine cortical bone

Hydroxyapatite powder was extracted from the bovine cortical bone according to the procedure which had been published by Bahrololoom et al.[55] Briefly, the spongy bones were removed, the cortical bone was de-fleshed, and the bone marrow and all pieces of meat and fat were cleaned. A gas torch was applied in order to burn the organic components of the bone by a direct flame. This thermal process generated some chars as a result of burning the organic components. To remove the remaining chars, the black powder was placed in a furnace at 800 °C for 3 h and was cooled inside the furnace. Following this process, the black bone ash changed to a white granular powder. A milling process was conducted on the prepared powder to reach the size of powder to around 1–5 μm.[55] 6 g chitosan was extracted from 50 g shrimp shells and 270 g HA from 500 g bovine cortical bone. Thus, the yields of chitosan and HA were 12 and 54%, respectively.

2.1.3. Preparation of CS/HA/magnetite nano-composites

The nano-composite preparation was performed according to the published report by Hu et al.[26] In this technique, $FeCl_2{\cdot}4H_2O$ and $FeCl_3{\cdot}6H_2O$ with the weight ratio of $FeCl_2{\cdot}4H_2O/FeCl_3{\cdot}6H_2O$ = 0.5 were

added to the solution of 2% (v/v) acetic acid under strong agitation for 30 min. Then, at room condition, the HA powder was mixed with the prepared solution and stirred for 1 h, which resulted in a homogeneous yellow solution. Subsequently, CS was added into the solution and vortexed for 1 h to prepare a yellow viscous solution.

In this step, a reaction between the chitosan and acetic acid occurs as below:[56]

$$CS-NH_2+CH3OOH\rightarrow CS-NH3++CH_3COO^-.$$

Eventually, the resulting solution was kept for 12 h in still condition for removal of air bubbles. The viscous solution of CS/HA/magnetite was casted into a mold. After soaking the it in a 5% (wt./v) NaOH solution for 12 h, a layer of gelatinous composite was formed on the surface of the molds.

The formation of this gelation layer and also magnetite nanoparticles are carried out according to following reactions [56]:

$$OH^-+CS-NH3+\rightarrow CS-NH_2+H_2O$$

$$Fe2++2Fe3++8OH^-\rightarrow Fe_3O_4+4H_2O.$$

Following the cleaning by distilled water, the pH of the composite's surface was around 7. The produced gel composites were placed in an oven at 60 °C for 24 h. Five specimens were produced for each test. For compression test, cylindrical specimens were produced with the diameter of 6.5 mm and the length of 13 mm. For bending test, rectangular specimens were produced with the length, width, and thickness of 75, 10, and 3.3 mm, respectively.

The amounts of the components for the preparation of CS/HA/magnetite nano-composites are presented in Table 1.

Table 1. The original amounts of the components for the preparation of HA/CS/magnetite nano-composite scaffolds.

Samples	CS (g)	HA (g)	$FeCl_2{\cdot}4H_2O$ (g)	$FeCl_3{\cdot}6H_2O$ (g)
CS	4	0	0	0

Samples	CS (g)	HA (g)	$FeCl_2 \cdot 4H_2O$ (g)	$FeCl_3 \cdot 6H_2O$ (g)
CS/HA	4	4	0	0
CS/HA/magnetite	4	4	0.5	1
CS/magnetite	4	0	0.5	1

2.2. Material characterization

2.2.1. Microstructural studies

Scanning electron microscope (SEM: S360 Cambridge) was utilized to characterize the morphology of the produced nano-composite materials and their fracture surfaces. The mounted samples on the aluminum stubs were gold coated to give required conductivity for good SEM imaging. The fracture surfaces were characterized using an image analyzer software. X-ray diffraction patterns (XRD: Bruker AXS D8 Discover) were recorded in the 2 theta range of 15–65° with scan speed of 0.01°/s.

2.2.2. Mechanical experiments

2.2.2.1. Bending tests

Bending test was performed by the three-point mode of a universal testing machine (Zwick/Roell Z020). The span length was 40 mm and the loading rate was 1 mm/min.

Bending strength (MPa) and bending modulus (GPa) were calculated using the values of Failure Load F (N), upper span L (mm), specimen width b (mm), thickness h (mm), and the tangent of the initial straight line of the load-deflection curve M (N/mm), according to Eqs. (1) and (2):

equation(1)

$$\text{Bendingstrength} : \frac{3FL}{\left(2bh^2\right)}$$

equation(2)

$$\text{Bendingmodulus} : \frac{\left(L^3M\right)}{\left(4bh^2\right)}.$$

Materials Science and Engineering C, Vol 65 (August 1, 2016): pg. 338-344. DOI.

Bending strength (MPa) and bending modulus (GPa) were calculated using the values of Failure Load F (N), upper span L (mm), specimen width b (mm), thickness h (mm), and the tangent of the initial straight line of the load-deflection curve M (N/mm), according to Eqs. (1) and (2):

equation(1)

$$\text{Bendingstrength} : \frac{3FL}{\left(2bh^2\right)}$$

equation(2)

$$\text{Bendingmodulus} : \frac{\left(L^3M\right)}{\left(4bh^2\right)}.$$

2.2.2.2. Compression tests

Compression test was conducted at a loading rate of 20 mm/min between parallel steel plates. Load versus displacement curves were recorded at a frequency of 100 Hz. Compressive strength (MPa) was calculated by dividing the Failure Load F (N) with the specimen cross-sectional area A (mm^2), in agreement with the ISO 5833 standard according to Eq. 3:

equation(3)

$$\text{Compressivestrength} : \frac{F}{A}.$$

2.2.2.3. Hardness tests

Hardness test was performed according to ASTM D2240-05 standard with hardness instrument type D (Shore D). Hardness number was determined after 15 second load relaxation and 5 kg indenter force.

2.2.3. Human Mesenchymal Stem Cell culture

Stem Pro® BM Mesenchymal Stem Cells isolated from human bone marrow were purchased from life technologies (Life Technologies-#A15652), cultured in Mesen PRO RS media in

humidified atmosphere of 5% CO_2, and maintained at 37 °C as per manufacturer's recommendations. Purchased cells of passage 4 (P4) were first subcultured in 75 cm^2 flasks, allowed to grow for 3 days and then transferred to a new 75 cm^2 flasks at a concentration of 4000 cell/cm^2. Cell culture media was replaced every two days. Flasks with the 80% cell confluence were washed in DPBS solution, trypsinized with TrypLE™ Select CTS™ reagent (Life Technologies), and washed again. Cells of passage 6 (P6) were utilized for all the experiments. Cell proliferation assays on different samples was measured using PrestoBlue Cell Viability Reagent (Life Technologies, USA). PrestoBlue® is a resazurin-based non-fluorescent reagent which is reduced by viable cells into fluorescent molecule resorufin. Briefly, the samples were sterilized with UV for 2 h and placed in 24-well low-attachment culture plates (1 sample/well in triplicates). The samples were soaked in 2 mL of growth medium for 2 h. Each sample was seeded with 8×10^4 cells in 1 mL of the cell suspension. Seeded samples were incubated with cell suspension overnight in a humidified atmosphere of 37 °C and 5% CO_2 to allow the cell attachment. Following the incubation, samples were washed twice with PBS solution to remove any unattached cells and moved into a new plate. The plates were incubated for a total of 7 days and Mesen PRO RS media was replaced every 2 days. The samples soaked in media without cells were employed as control groups. After 7 days incubation, 100 μL of PrestoBlue reagent was added to each well and these plates were incubated for an additional 2 h. The contents of each well were mixed with pasture pipette for uniform distribution of color. About 200 μL of the solution was transferred to 96 well plates; fluorescence was measured with emission and excitation wavelengths of 560 nm and 590 nm, respectively, in a spectrophotometer. Total number of attached viable cells to samples was determined by using a standard curve. Standard curve was generated by aliquoting cells into a 96-well plate within the range of 10,000–200,000 cells/well. After 8 h incubation with the purpose of helping the cells to attach to the plate, cell viability was measured using the above mentioned kit as per manufacturer's recommendations. A standard curve was generated by plotting number of cells versus fluorescence. The samples soaked in media without cells were employed as the control group. The cell viabilities were stated as OD_{sample} / $OD_{control}$ × 100%, in which OD_{sample}

Materials Science and Engineering C, Vol 65 (August 1, 2016): pg. 338-344. DOI.

and $OD_{control}$ are the optical density (absorbance) of the samples and the control, respectively.

3. Results and discussion

3.1. Microstructural studies

The SEM image of extracted chitosan from shrimp shells and extracted HA from bovine cortical bone has been presented in Fig. 1. Also, the size of the magnetite nanoparticles was around 10–40 nm with irregular shapes.[52] Fig. 2 shows the cross-sectional SEM images of CS (a), CS/HA (b), CS/HA/magnetite (c), and CS/magnetite (d) samples. According to these figures, CS/HA/magnetite (Fig. 2c) and CA/magnetite (Fig. 2d) have the lesser porosity than the CS (Fig. 2a) and CS/HA (Fig. 2b) due to the existence of magnetite nano-particles which have precipitated with in situ technique into the CS matrix. SEM images show that HA particles have been uniformly dispersed in the CS/HA (Fig. 2b) and CS/HA/magnetite matrix (Fig. 2c). Note that although nano-sized magnetite is not observable in the present magnification of SEM images, its influence on CS/HA/magnetite and CS/magnetite samples was notable. The samples containing magnetite nano-particles presented a smooth surface without the cracks as a result of precipitation of magnetite particles.

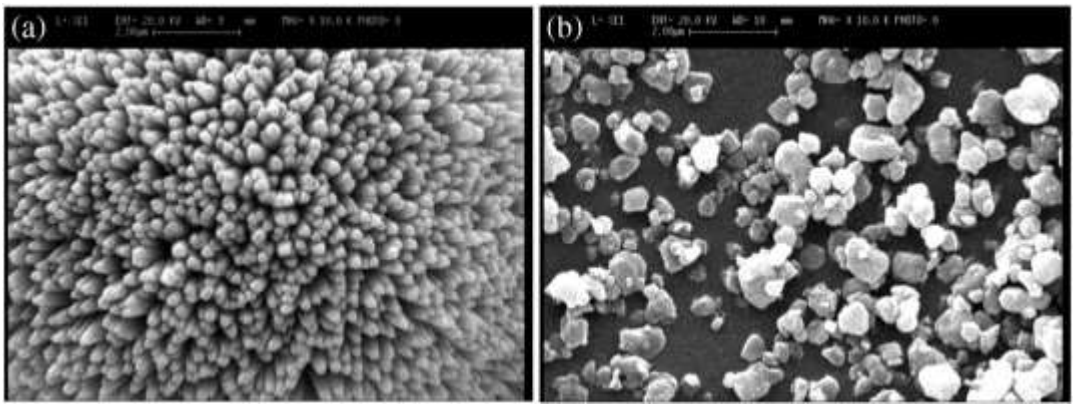

Fig. 1. SEM images of extracted chitosan from shrimp shells (a) and extracted HA from bovine cortical bone (b).

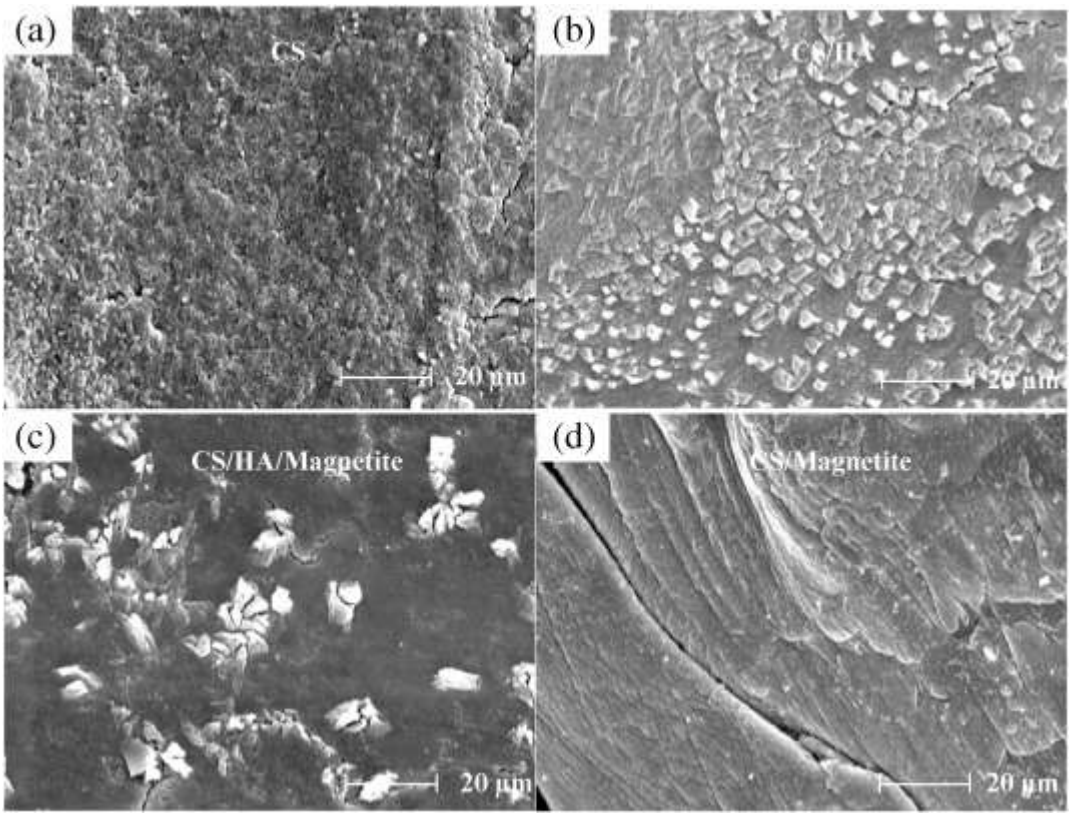

Fig. 2. Cross-sectional SEM images of CS (a), CS/HA (b), CS/HA/magnetite (c) and CS/magnetite (d) samples.

Fig. 3 shows the XRD patterns of the produced HA, CS/magnetite, and CS/HA/magnetite composites. According to the XRD pattern of HA, the characteristic peaks of HA are observed in the pattern. The XRD pattern of CS/magnetite is also confirming the formation of Fe_3O_4 phase in the peaks with the 2 theta of 30, 35.6, 46.7, 48, 53.7, and 62.5°. In CS/HA/magnetite, beside the HA peaks, Fe_2O_3 and Fe_3O_4 phases were detected in 45.5 and 46.7°.

Materials Science and Engineering C, Vol 65 (August 1, 2016): pg. 338-344. DOI.

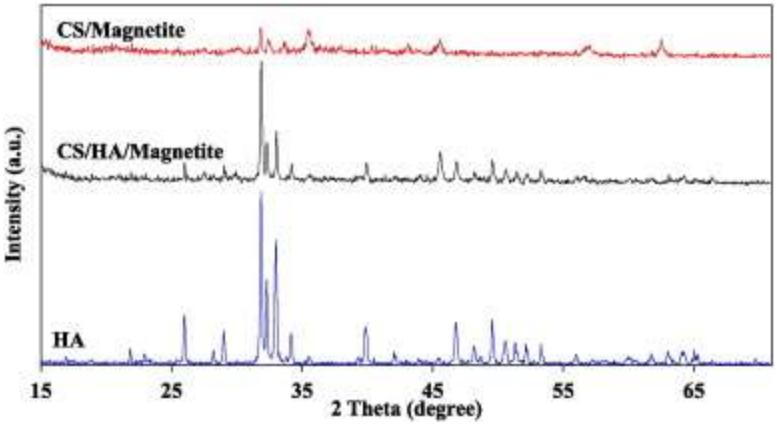

Fig. 3. Comparison of the XRD patterns of the produced HA, CS/magnetite and CS/HA/magnetite composite.

Since there is no chemical reaction for the formation of CS and HA, the real content of CS and HA in the final composite (CS/HA/magnetite) is same with the initial used materials, however, the magnetite phase is formed as the result of a chemical reaction between the $FeCl_2 \cdot 4H_2O$ and $FeCl_3 \cdot 6H_2O$ (g). Thus, determination of real content of magnetite in the final composite demands more analytical studies.

Fig. 4 shows the SEM micrographs (a, b, c, d) and confocal images (e, f, g, h) from the cross-sectional view of CS (a), CS/HA (b), CS/HA/magnetite (c), and CS/magnetite (d) indicating the cracks and porosities in the fracture surface of samples after bending test. According to Fig. 4a, some cracks could be observed indicating that the fracture surface of CS is brittle. Fig. 4b shows that HA particles in the CS matrix inhibited crack growth in the CS/HA composite since all cracks has been formed in the vicinity of HA leading to the crack deflection. It is worth noting that the submicron size of HA particles in CS/HA composite caused the smaller distance for crack growth indicating a rough surface according to Fig. 4b. CS/HA/magnetite composite requires much activation energy for crack growth and ultimate fracture owing to the existence of magnetite nano-particles (Fig. 4c). According to Fig. 4d, CS/magnetite composite shows a smooth surface without brittle fracture when compared with CS in Fig. 4a. Fig. 4e–h are images of a confocal image analyzer. In these images, the defects including the crack growth and porosities in cross sections of samples were represented more clearly. Crack track and porosity in the CS/HA composite (Fig. 4f) are much more than others.

Materials Science and Engineering C, Vol 65 (August 1, 2016): pg. 338-344. DOI.

More porosities could be detected in the CS (Fig. 4e) compared to that of the CS/magnetite (Fig. 4h). Although, CS/HA (Fig. 4f) and CS/HA/magnetite (Fig. 4g) have similar contents of HA, lesser amount of cracks is observed in the CS/HA/magnetite due to the existence of magnetite nano-particle precipitations.

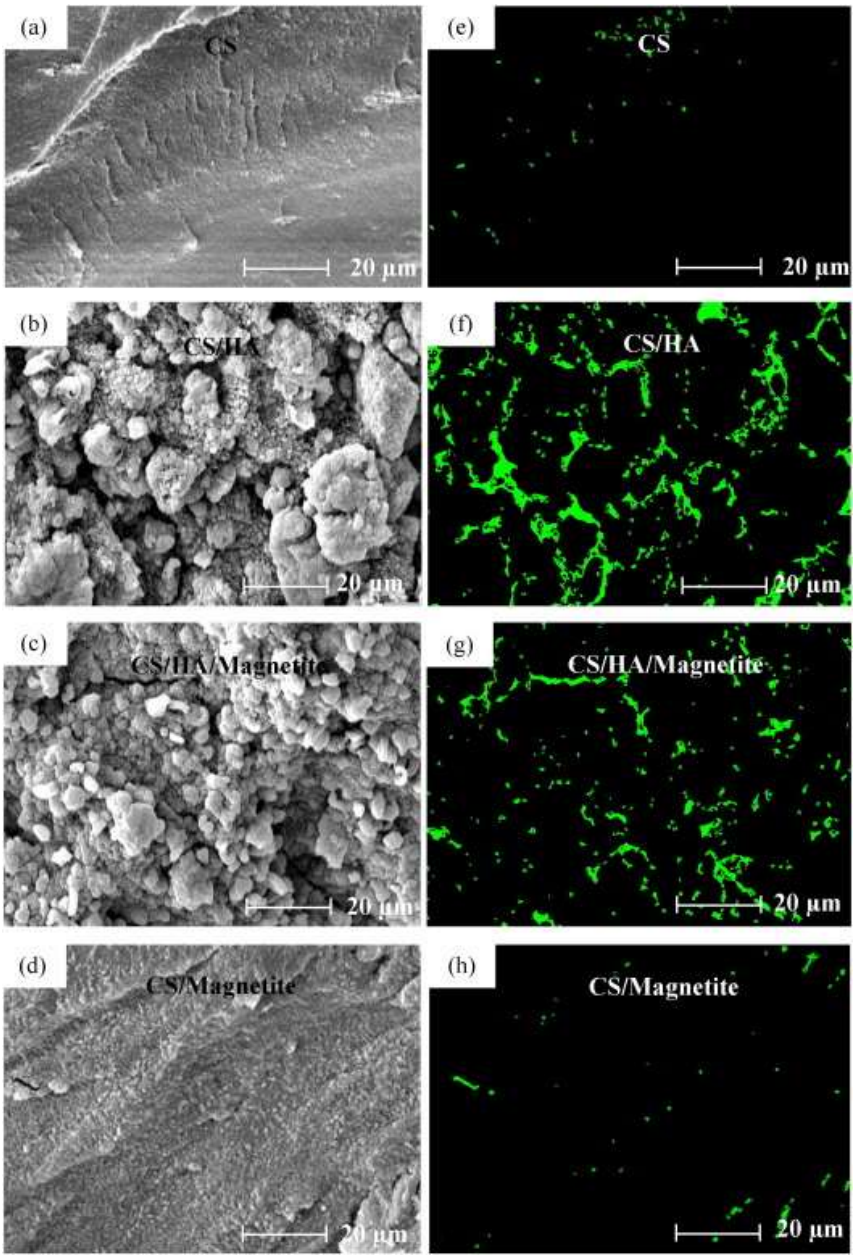

Fig. 4. SEM micrographs (a, b, c, d) and confocal images (e, f, g, h) from the cross-sectional view of CS (a), CS/HA (b), CS/HA/magnetite (c), and CS/magnetite (d) indicating the cracks and porosities in the fracture surface of samples after bending test.

3.2. Bending tests

Bending stress-strain curves for the CS, CS/HA, CS/HA/magnetite, and CS/magnetite have been presented in Fig. 5 and the relevant outputs including bending strength, bending modulus, and bending toughness have been summarized in Table 2. As can be observed in Table 2, adding the HA and magnetite particles to the CS matrix can enhance both bending strength and modulus. However, addition of HA decreases the bending toughness. The maximum bending strength is attributed to the CS/magnetite samples (34 MPa). CS/HA samples have the highest bending modulus (2.6 GPa) amongst all groups, while CS/magnetite presented the maximum bending toughness (0.66). CS/HA/magnetite samples have lower bending strength and bending toughness compare to CS/HA samples. This might be due to the agglomeration of magnetite nano-particles at the presence of HA particles which prevents CS to act as an appropriate binder matrix for the ceramic phases.

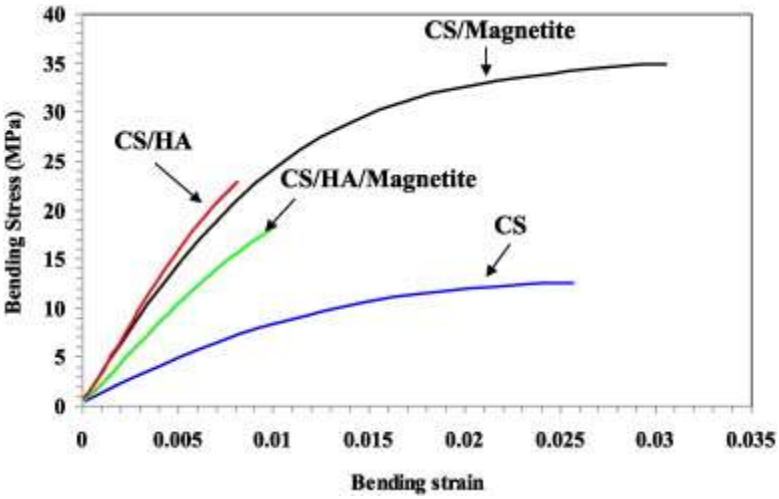

Fig. 5. Bending stress-strain curves for the CS, CS/HA, CS/HA/magnetite, and CS/magnetite samples.

Table 2. Bending strength, bending modulus and bending toughness of CS, CS/HA, CS/HA/magnetite, and CS/magnetite.

Samples	Bending strength (MPa)	Bending modulus (GPa)	Bending toughness (MJ/m^3)
CS	12.5 ± 3.1	0.7 ± 0.3	0.14 ± 0.03
CS/HA	27.7 ± 3.2	2.6 ± 1.3	0.09 ± 0.01
CS/HA/magnetite	17.6 ± 2.5	1.9 ± 0.9	0.09 ± 0.02

Samples	Bending strength (MPa)	Bending modulus (GPa)	Bending toughness (MJ/m^3)
CS/magnetite	34.8 ± 1.9	2.3 ± 1.3	0.66 ± 0.1

Incorporation of HA into the CS matrix via blending technique decreases the mechanical properties of CS/HA composite due to the weak interfacial bonding between HA filler and CS matrix.[57]

Previous researches showed that the ratio of CS/HA plays an important role in improvement of mechanical properties of this type of composites.[44] Human bone has a bending strength of 100–150 MPa, compressive strength of 2–10 MPa and the bending modulus of 7–25 GPa.[43,58] Through the blending technique for the production of CS/HA/magnetite nanocomposite in our research, it was not possible to reach to the range of bending strength of human bone, which we suspect is due to the difference between the particle size of extracted HA and that of the natural bone.

According to Fig. 5 and in view of the area under the curves corresponding to toughness, CS/magnetite has the highest toughness and bending strength. The existence of magnetite nano-particles may be the reason of this fact and by the same basis, CS/HA/magnetite possess lesser modulus than that of the CS/HA.

3.3. Compression tests

Fig. 6 exhibits the compression stress-strain curves of CS, CS/HA, CS/HA/magnetite, and CS/magnetite samples. The related outputs including compressive strength, compressive modulus, and compressive toughness have been summarized in Table 3. As can be observed in Table 3, addition of HA and magnetite particles to the CS matrix can improve both the compression strength and modulus while it can reduce the compressive toughness. Adding the HA particles into the CS matrix enhanced its compressive strength. Owing to the same amount of HA particles in the CS matrix for the CS/HA and CS/HA/magnetite, a little difference in their compressive strength has been detected but the amount of strain for the CS/HA/magnetite sample was lesser than that of the CS/HA sample. This may be due to the existence of HA particles which can act as the inhibitor phase for the precipitation of magnetite into the CS matrix preventing the

Materials Science and Engineering C, Vol 65 (August 1, 2016): pg. 338-344. DOI.

adhesion between the CS and ceramic phases including the HA and magnetite. Furthermore, CS/HA/magnetite and particularly CS/magnetite samples presented the most compressive strength compared to others which may be caused by the presence of magnetite precipitates in the CS matrix.

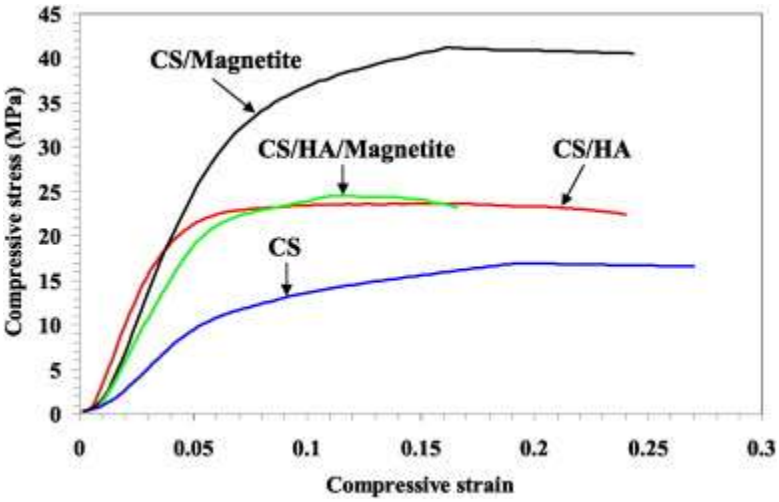

Fig. 6. Compression stress-strain curves of CS, CS/HA, CS/HA/magnetite, and CS/magnetite samples.

Table 3. Compressive strength, compressive modulus and compressive toughness of CS, CS/HA, CS/HA/magnetite, and CS/magnetite.

Samples	Compressive strength (MPa)	Compressive modulus (GPa)	Compressive toughness (MJ/m^3)
CS	16.9 ± 1.1	0.2 ± 0.1	3.4 ± 0.4
CS/HA	23.6 ± 2.1	0.6 ± 0.1	4.8 ± 0.3
CS/HA/magnetite	24.5 ± 2.4	0.3 ± 0.1	3.0 ± 0.2
CS/magnetite	41.1 ± 2.6	0.6 ± 0.1	7.7 ± 0.2

According to Table 3, an increase in compressive strength was observed due to the existence of magnetite nano-particles. Several factors such as particle size and distribution of HA and magnetite particles, mechanical properties of chitosan, interfacial interactions between chitosan, HA and magnetite can contribute in altering the mechanical properties.[59]

3.4. Hardness tests

The results of hardness test on the CS, CS/HA, CS/HA/magnetite, and CS/magnetite have been presented in Fig. 7. According to this figure, CS/magnetite sample has more hardness compared to that of the CS, CS/HA, and CS/HA/magnetite. Although, both of the CS and HA are the hard materials, precipitation of the magnetite nano-particles in CS matrix has made the material harder. For the same reason, CS/HA/magnetite is harder than CS/HA sample.

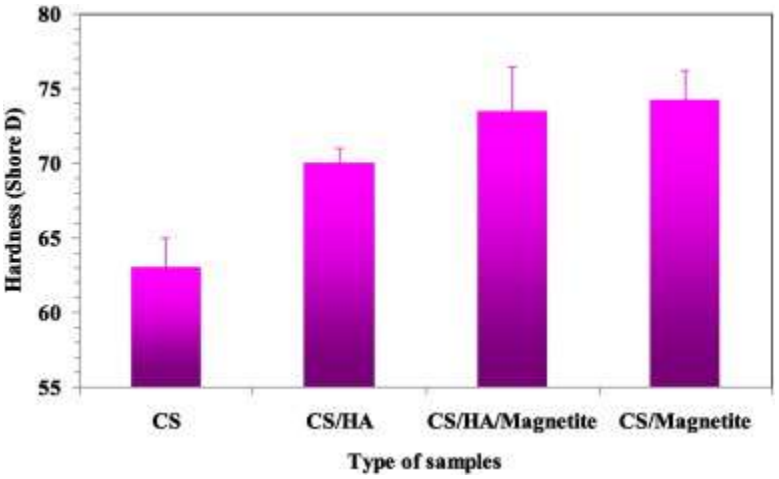

Fig. 7. The results of hardness test on the CS, CS/HA, CS/HA/magnetite, and CS/magnetite samples.

3.5. In vitro biocompatibility

The cell viability was expressed as the number of cells per unit surface on different scaffolds after 7 days of culturing. Fig. 8 shows the cell viability (% of control) of human Mesenchymal Stem Cells after 7 days of culture on different samples (CS, CS/HA, CS/HA/magnetite, and CS/magnetite). It is known that CS is highly biocompatible and as can be seen in this figure. the number of viable cells in CS sample is more than others. However, the number of cells is not that might lower in other samples to prove any toxicity. Basically, we can conclude that all these samples are biocompatible with little difference on their capability for cell attachment. It is important to note that the results indicated that having magnetic nano-particle does not have reverse effect on the in vitro biocompatibility of samples. Future research trends mainly focus on the in-depth study of biocompatibility

of developed composites using different cell types and providing phase contrast images of the cells during the treatment process to validate the morphological changes.

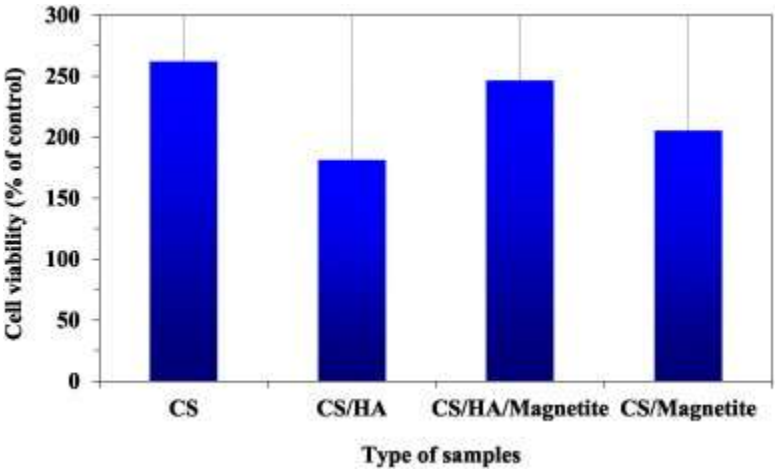

Fig. 8. Cell viability (% of control) of human Mesenchymal Stem Cells after 7 days of culture on different samples (CS, CS/HA, CS/HA/magnetite, and CS/magnetite).

4. Conclusion

This study examined the mechanical and cyto-compatibility properties of CS, CS/HA, CS/magnetite, and CS/HA/magnetite samples synthesized from the natural HA and CS extracted from the bone and shrimp shells, respectively. CS/magnetite presented the maximum bending strength (34 MPa) while CS/HA had the highest bending modulus (2.6 GPa). Compare to the CS/HA, CS/HA/magnetite presented lesser bending strength and bending toughness. Bending surface fracture micrographs showed that fracture of CS and CS/HA was more brittle than that of CS/HA/magnetite and CS/magnetite. CS/magnetite offered the highest compressive strength (41.06 MPa) compared to other samples which may be due to the existence of magnetite particles in the CS matrix. Although both of the CS and HA are the hard materials, precipitation of the magnetite nano-particles in CS matrix has hardened the material more effectively. Therefore, CS/HA/magnetite was harder than CS/HA sample. Probable agglomeration of magnetite nano-particles at the presence of HA particles may have a role in obtaining this result as it can prevent CS to perform as a suitable binder matrix for the ceramic phases. The number of viable cells in CS sample is more than others. However, the number of cells in other samples is not too low to evidence any

toxicity. Thus, we conclude having magnetic nano-particles does not have reverse effect on the cyto-compatibility of samples.

Acknowledgement

The authors are thankful of the support from the Research Committee of Shiraz University (grant no. 86-GR-ENG-62 to M.E. Bahrololoom), Delta Dental, National Science Foundation (NSF, grant no. EEC-1160483, ECCS-1351533 and CMMI-1363485), AFOSR under contract number FA9550-12-1-0225, and Marquette University Strategic Innovation Fund.

References

[1]H.H. De Boer. *Clin. Orthop. Relat. Res.,* 226 (1988), pp. 292–298

[2]M. Yazdimamaghani, T. Pourvala, E. Motamedi, B. Fathi, D. Vashaee, L. Tayebi. Materials, 6 (2013), pp. 3727–3741

[3]E. Salahinejad, M.J. Hadianfard, D.D. Macdonald, I. Karimi, D. Vashaee, L. Tayebi. *Ceram. Int.,* 38 (2012), pp. 6145–6149

[4]M. Yazdimamaghani, D. Vashaee, S. Assefa, M. Shabrangharehdasht, A.T. Rad, M.A. Eastman, K.J. Walker, S.V. Madihally, G.A. Köhler, L. Tayebi. *Mater. Sci. Eng. C,* 39 (2014), pp. 235–244

[5]P. Rouhani, E. Salahinejad, R. Kaul, D. Vashaee, L. Tayebi. *J. Alloys Compd.,* 568 (2013), pp. 102–105

[6]E. Salahinejad, M. Hadianfard, D. Macdonald, M. Mozafari, D. Vashaee, L. Tayebi. *Ceram. Int.,* 39 (2013), pp. 1271–1276

[7]E. Salahinejad, M. Hadianfard, D. Macdonald, I. Karimi, D. Vashaee, L. Tayebi. *Ceram. Int.,* 38 (2012), pp. 6145–6149

[8]M. Razavi, M.H. Fathi, O. Savabi, D. Vashaee, L. Tayebi. *Phys. Sci. Int. J.,* 4 (2014), pp. 708–722

[9]M. Yazdimamaghani, M. Razavi, D. Vashaee, L. Tayebi. *Mater. Sci. Eng. C,* 49 (2015), pp. 436–444

[10]M. Razavi, M. Fathi, O. Savabi, D. Vashaee, L. Tayebi. *Mater. Sci. Eng. C,* 48 (2015), pp. 21–27

[11]E. Salahinejad, M. Hadianfard, D. Macdonald, M. Mozafari, D. Vashaee, L. Tayebi. *Mater. Lett.,* 88 (2012), pp. 5–8

[12]M. Razavi, M. Fathi, O. Savabi, S.M. Razavi, F. Heidari, M. Manshaei, D. Vashaee, L. Tayebi. *Appl. Surf. Sci.,* 313 (2014), pp. 60–66

[13]M. Mozafari, D. Vashaee, L. Tayebi, M. Mehraien. *Electroconductive Nanocomposite Scaffolds: A New Strategy Into Tissue Engineering and Regenerative Medicine*. INTECH Open Access Publisher (2012)

[14]S.M. Rabiee, N. Nazparvar, M. Azizian, D. Vashaee, L. Tayebi. *Ceram. Int.,* 41 (2015), pp. 7241–7251

[15]M. Razavi, M. Fathi, O. Savabi, B. Hashemi Beni, D. Vashaee, L. Tayebi. *Ceram. Int.,* 40 (2014), pp. 9473–9484

[16]M. Yazdimamaghani, M. Razavi, D. Vashaee, L. Tayebi. *Mater. Lett.,* 132 (2014), pp. 106–110

[17]M. Razavi, M. Fathi, O. Savabi, D. Vashaee, L. Tayebi. *Mater. Sci. Eng. C,* 41 (2014), pp. 168–177

[18]A. Ghafari-Nazari, F. Moztarzadeh, S.M. Rabiee, T. Rajabloo, M. Mozafari, L. Tayebi. *Ceram. Int.,* 38 (2012), pp. 5445–5451

[19]M. Razavi, M. Fathi, O. Savabi, D. Vashaee, L. Tayebi. *Surf. Interface Anal.,* 46 (2014), pp. 387–392

[20]P.J. VandeVord, H.W. Matthew, S.P. DeSilva, L. Mayton, B. Wu, P.H. Wooley. *J. Biomed. Mater. Res.,* 59 (2002), pp. 585–590

[21]J.-Y. Lee, S.-H. Nam, S.-Y. Im, Y.-J. Park, Y.-M. Lee, Y.-J. Seol, C.-P. Chung, S.-J. Lee. *J. Control. Release,* 78 (2002), pp. 187–197

[22]E. Khor, L.Y. Lim. *Biomaterials*, 24 (2003), pp. 2339–2349

[23]S.V. Madihally, H.W. Matthew. *Biomaterials*, 20 (1999), pp. 1133–1142

[24]A. Di Martino, M. Sittinger, M.V. Risbud. *Biomaterials*, 26 (2005), pp. 5983–5990

[25]K. Gupta, M.N.R. Kumar. *J. Mater. Sci. Mater. Med.,* 12 (2001), pp. 753–759

[26]Q.-l. Hu, Z.-p. Fang, Y. Zhao, C.-w. Xu. 高分子科学, 19 (2001), pp. 467–470

[27]Q. Hu, X. Qian, B. Li, J. Shen. *Chem. J. Chin. Univ.,* 24 (2002), pp. 528–531

[28]D.M. Roy, S.K. Linnehan, (1974).

[29]G. Wei, P.X. Ma. *Biomaterials*, 25 (2004), pp. 4749–4757

[30]B. Leukers, H. Gülkan, S.H. Irsen, S. Milz, C. Tille, M. Schieker, H. Seitz. *J. Mater. Sci. Mater. Med.,* 16 (2005), pp. 1121–1124

[31]M. Kuo, S. Yen. *Mater. Sci. Eng. C*, 20 (2002), pp. 153–160

[32]M. Akao, H. Aoki, K. Kato. *J. Mater. Sci.,* 16 (1981), pp. 809–812

[33]J.R. Woodard, A.J. Hilldore, S.K. Lan, C. Park, A.W. Morgan, J.A.C. Eurell, S.G. Clark, M.B. Wheeler, R.D. Jamison, A.J.W. Johnson. *Biomaterials*, 28 (2007), pp. 45–54

[34]S. Baradaran, E. Moghaddam, W. Basirun, M. Mehrali, M. Sookhakian, M. Hamdi, M.N. Moghaddam, Y. Alias. *Carbon*, 69 (2014), pp. 32–45

[35]O.C. Wilson, J.R. Hull. *Mater. Sci. Eng. C,* 28 (2008), pp. 434–437

[36]Y. Wan, Y. Huang, C. Yuan, S. Raman, Y. Zhu, H. Jiang, F. He, C. Gao. *Mater. Sci. Eng. C,* 27 (2007), pp. 855–864

[37]X. Wang, J. Ma, Y. Wang, B. He. *Biomaterials*, 23 (2002), pp. 4167–4176

[38]T. Ang, F. Sultana, D. Hutmacher, Y.S. Wong, J. Fuh, X. Mo, H.T. Loh, E. Burdet, S.-H. Teoh. *Mater. Sci. Eng. C,* 20 (2002), pp. 35–42

[39]C. Xianmiao, L. Yubao, Z. Yi, Z. Li, L. Jidong, W. Huanan. *Mater. Sci. Eng. C,* 29 (2009), pp. 29–35

[40]D. Verma, K.S. Katti, D.R. Katti, B. Mohanty. *Mater. Sci. Eng. C,* 28 (2008), pp. 399–405

[41]S.N. Danilchenko, O.V. Kalinkevich, M.V. Pogorelov, A.N. Kalinkevich, A.M. Sklyar, T.G. Kalinichenko, V.Y. Ilyashenko, V.V. Starikov, V.I. Bumeyster, V.Z. Sikora. *J. Biomed. Mater. Res. A,* 96 (2011), pp. 639–647

[42]S.H. Teng, E.J. Lee, B.H. Yoon, D.S. Shin, H.E. Kim, J.S. Oh. *J. Biomed. Mater. Res. A,* 88 (2009), pp. 569–580

[43]X.-m. Pu, K. Wei, Q.-q. Zhang. *Mater. Lett.,* 94 (2013), pp. 169–171

[44]Q. Hu, B. Li, M. Wang, J. Shen. *Biomaterials*, 25 (2004), pp. 779–785

[45]M.L. Spence, M.G. McCord. Biomedical Engineering Conference, 1997. *Proceedings of the 1997 Sixteenth Southern, IEEE (1997),* pp. 257–259

[46]X. Cai, H. Tong, X. Shen, W. Chen, J. Yan, J. Hu. *Acta Biomater.,* 5 (2009), pp. 2693–2703

[47]H. Zhao, H. Jin, J. Cai. *Mater. Lett.,* 116 (2014), pp. 293–295

[48]Z. Hong, P. Zhang, C. He, X. Qiu, A. Liu, L. Chen, X. Chen, X. Jing. *Biomaterials*, 26 (2005), pp. 6296–6304

[49]K. Donadel, M.D. Felisberto, V.T. Fávere, M. Rigoni, N.J. Batistela, M.C. Laranjeira. *Mater. Sci. Eng. C,* 28 (2008), pp. 509–514

[50]A.M. Grumezescu, E. Andronescu, A. Ficai, C. Bleotu, D.E. Mihaiescu, M.C. Chifiriuc. *Int. J. Pharm.,* 436 (2012), pp. 771–777

[51]M. Ghaemy, M. Naseri. *Carbohydr. Polym.,* 90 (2012), pp. 1265–1272

[52]F. Heidari, M.E. Bahrololoom, D. Vashaee, L. Tayebi. *Ceram. Int.,* 41 (2015), pp. 3094–3100

[53]R. Bazargan-Lari, M. Bahrololoom, A. Nemati. *J. Food Agric. Environ.,* 9 (2011), pp. 892–897

[54]S. Sabnis, L.H. Block. *Polym. Bull.,* 39 (1997), pp. 67–71

[55]M. Bahrololoom, M. Javidi, S. Javadpour, J. Ma, J. Ceram. *Proteome Res.,* 10 (2009), pp. 129–138

[56]Q. Hu, F. Chen, B. Li, J. Shen. *Mater. Lett.,* 60 (2006), pp. 368–370

[57]B.-Q. Li, Q.-L. Hu, X. Qian, Z. Fang, J. Shen. *Acta Polym. Sin.,* 6 (2002), pp. 828–833

[58]D.W. Hutmacher. *Biomaterials*, 21 (2000), pp. 2529–2543

[59]M. Nikpour, S. Rabiee, M. Jahanshahi. *Compos. Part B,* 43 (2012), pp. 1881–1886

Corresponding author at: Department of Developmental Sciences, Marquette University School of Dentistry, Milwaukee, WI 53233, USA.